Program Digest, 2019 IEEE International Ultrasonics Symposium (IUS)
Glasgow, Scotland, October 6-9, 2019

Improving Harmonic Motion Estimation with Phase-Based Estimators for Magnetomotive Ultrasound Imaging

Tim C. Kranemann, Thomas Ersepke, and Georg Schmitz
Chair for Medical Engineering
Ruhr University Bochum
Bochum, Germany
{tim.kranemann, thomas.ersepke, georg.schmitz}@rub.de

***Abstract*—Magnetomotive Ultrasound Imaging relies on estimates of the harmonic motion in tissue from ultrasound data. It was shown that data containing harmonic motion are different in spectral content from those containing uniform motion as in classical Doppler methods. However, common computationally efficient phase-based motion estimators are similar to Doppler processing. Simulation data indicate that even in case of noise-free data, the phase-based estimators exhibit a significant error in a typical magnetomotive ultrasound scenario. An improvement of the estimator, measured as a reduction of over 50 % in mean absolute error, was achieved in the simulation scenario by pre-filtering radio frequency data components not associated with motion and reducing the bandwidth of radio frequency data or by averaging motion estimates obtained in different frequency bands. Thereby, it was shown that a substantial improvement of the estimators is possible without increasing the computational effort significantly. However, it was also pointed out that further improvement in case of small harmonic displacements ratio seems possible only with different estimators derived from more sophisticated signal models.**

***Index Terms*—Doppler processing, harmonic motion, magnetic nanoparticles, magnetomotive ultrasound imaging, motion estimation, signal processing.**

I. Introduction

In magnetomotive (MM) ultrasound imaging (US), magnetic nanoparticles (MNP) are visualized by motion estimation in US data. Motion is induced by a magnetic field that exerts a force on the MNPs which are embedded in tissue. If the excitation is a sinusoidally varying magnetic field, the force is typically also harmonic which leads to a harmonic tissue motion at the known frequency of magnetic excitation. It is desired to estimate amplitude and phase of the motion spatially resolved since from this motion map the MNP distribution or prospectively MNP concentration or mechanical tissue properties can be reconstructed. Hence, by administering MNPs to the respective imaging region, MMUS offers the potential for molecular imaging and to obtain different parameters that are not accessible in standard US. However, the estimation of small displacements between 0.01–$100\,\mu\mathrm{m}$ is challenging.

With regard to signal processing, two characteristics are typical for MMUS and harmonic motion estimation in ultrasonic data: First, the motion is harmonic at a known frequency, which implies that the tissue is in its original configuration after a period of magnetic excitation, if no superimposed interfering motion was present. This distinguishes MMUS from Doppler methods that perform speckle tracking for the visualization of flow. Second, motion must be usually estimated on a speckle pattern, as the tiny MNPs are well below the resolution limit of US.

Magnetomotive ultrasound imaging was introduced in 2006 [1] and performed with standard Doppler modes that are available on clinical scanners. Surprisingly, these can indicate merely the presence of vibrating MNPs. Previously, a different technique for optical coherence tomography (OCT) was proposed [2]. There, amplitude variations in the typical B-mode data were used for motion detection. In OCT [3], it was early made use of the phase of the complex in-phase and quadrature (IQ)-data for MM motion estimation. Later in MMUS, a cross-correlation tracking approach has been implemented [4]. The amplitude variation of the RF data was used to improve the phase-based estimation [5]. Amplitude and phase of the motion in MMUS was calculated in [6] based on the phase of the IQ-data and used to suppress motion outside the MNP loaded region. This is considered to be the standard method currently used in MMUS. Also in OCT, this method was adapted [7]. Hence, the majority of publications in the field of MMUS work with the relatively simple phase-based motion estimation technique, with the advantage of being real-time capable [8].

To further enhance the sensitivity of MMUS, e. g., to reduce the tracer concentration or magnetic field strength, a preprocessor was suggested in [9]. We have previously implemented a time-domain motion estimator using a Bayesian framework [10] and compared it to a phase-based method following [6]. The results showed that better motion estimations can be achieved than with the conventional phase-based method. However, time-domain estimators are often computationally more demanding than the currently used phase-based variants. Therefore, the further development of phase-based methods is of particular interest. Here, an improvement of the phase-

This work is funded by the German Federal Ministry of Education and Research, contract number 13GW0069B (project SAMBA-PATI).

based estimators is approached by formulating a signal model of US data with harmonic motion. Deficiencies of the conventional estimator are improved by preprocessing the ultrasound data before estimation or averaging estimates. A significant improvement of a phase-based estimator with minimal modifications is thereby demonstrated in a simulation scenario.

II. Methods

A. Ultrasound simulation

Ultrasound radio frequency (RF) data of a single A-scan was generated with the Field II US simulation toolbox [11]. A transducer with center frequency $f_0 = 8\,\mathrm{MHz}$ and approx. $100\,\%$ bandwidth with a Gaussian shaped power density spectrum was used. The simulation was performed at a sampling frequency of $128\,\mathrm{MHz}$ and RF data were downsampled to $f_s = 4 f_0$ which is a typical sampling frequency of an US system. The transducer aperture consisted of 67 elements of $170\,\mathrm{\mu m}$ width separated by a $30\,\mathrm{\mu m}$ kerf. It was focused to a depth of $z_{\mathrm{foc}} = 20\,\mathrm{mm}$ on transmit. On receive, a dynamic focusing was used to achieve a homogeneous point-spread-function in the field of view. The RF data generated represent an axial line of a B-mode image.

As a tissue model, a uniform distribution of 20 scatterers per resolution was created. The resolution cell was calculated as a volume of $2\,\lambda^3$ via the wavelength at center frequency $\lambda = c/f_0$ and with the background speed of sound $c = 1540\,\mathrm{m\,s^{-1}}$. The tissue phantom is centered around the focus of the aperture and has a dimension of $20\,\mathrm{mm}$ (axial) $\times$ $4\,\mathrm{mm}$ (lateral) $\times$ $750\,\mathrm{\mu m}$ (elevational), the latter being $1/10$ of the respective transducer dimension.

The simulation of RF data was repeated with a frame rate of $f_F = 2\,\mathrm{kHz}$ while all scatterers are axially moved with a motion amplitude distribution with a Gaussian profile, sinusoidally varying over the slow time t. This displacement profile with a peak displacement of $\xi_0 = 5\,\mathrm{\mu m}$ is

$$\xi(z,t) = \underbrace{\xi_0 \, \exp\left(-\frac{(z-z_0)^2}{2\,\sigma_z^2}\right)}_{\xi(z)} \underbrace{\sin(\omega_{\mathrm{M}}\, t)}_{\xi(t)} \,, \tag{1}$$

and with $\sigma_z = 5/3\,\mathrm{mm}$, the motion frequency $f_{\mathrm{M}} = 20\,\mathrm{Hz}$ and $\omega_{\mathrm{M}} = 2\pi\, f_{\mathrm{M}}$. Simulations were performed for one motion period, i. e., 100 frames. The RF data for a measurement of $1\,\mathrm{s}$ were composed from this. Uncorrelated white Gaussian noise was added to the RF data to get different signal-to-noise ratios (SNRs) with the powers calculated over the entire RF dataset.

B. Signal model

The RF signal is a function of the fast time t_f, corresponding to the axial dimension, which is here expressed as the space variable $z = c\,t_f/2$, and of the slow time t as in (1). The velocity of motion in MMUS is at least three orders of magnitude slower than the speed of sound even if an unrealistic displacement of $500\,\mathrm{\mu m}$ at a motion frequency of $500\,\mathrm{Hz}$ is considered. This motivates to neglect spectral distortions due to Doppler effects and view a single scan over the fast time as a snapshot of the tissue configuration.

The RF data or A-scan at reference slow time $t_0 = 0$ is

$$e_{\mathrm{ref}}(z) = s_{\mathrm{t}}(z) \, * \, u_{\mathrm{ref}}(z) \,. \tag{2}$$

It is generated by convolution of the physical, i. e., band-pass, high-frequency ultrasound pulse $s_{\mathrm{t}}(z)$ with the impulse response of the tissue $u_{\mathrm{ref}}(z)$ in mechanical reference configuration. The latter is a white process when speckle is fully developed. Hence, the A-scan is a band-pass signal around f_0, i. e., the Fourier-transform with respect to fast time z is

$$E_{\mathrm{ref}}(k_z) = \mathcal{F}_z\left\{e_{\mathrm{ref}}(z)\right\} = S_{\mathrm{t}}(k_z)\, U_{\mathrm{ref}}(k_z) \tag{3}$$

and contains all energy in the passband of the transducer.

Motion relative to the reference configuration

$$u(z,t) = u_{\mathrm{ref}}(g(z,t)) \,, \tag{4}$$

is introduced with $g(z,t)$ that is in MMUS typically

$$g(z,t) = z - \xi(z)\, \sin(\omega_{\mathrm{M}}\, t + \varphi_{\mathrm{M}}(z)) \,. \tag{5}$$

Signal processing for MMUS can hence be defined as estimating $\xi(z)$ and $\varphi_{\mathrm{M}}(z)$ from noisy A-scan observations

$$e(z,t) = s_{\mathrm{t}}(z) \, * \, u(z,t) + n(z,t) \,, \tag{6}$$

with the uncorrelated white Gaussian noise process $n(z,t)$.

C. Conventional phase-based motion estimator

Although the signal model (6) is easy to formulate, it is difficult to derive an estimator from it. Therefore, the standard approach, here according to the concept of [6], is to generate the IQ signal by demodulation with the center frequency of the ultrasonic pulse and filtering with the low-pass filter $h(z)$

$$e_{\mathrm{IQ}}(z,t) = \left(e(z,t)\,\mathrm{e}^{\mathrm{j}\frac{4\pi}{\lambda}z}\right) \, * \, h(z) \,. \tag{7}$$

Its phase is defined as the argument of the IQ data

$$\Phi(z,t) = \arg\left\{e_{\mathrm{IQ}}(z,t)\right\} \,, \tag{8}$$

where unwrapping must be performed if necessary. Thereof, the complex motion estimate is obtained by Fourier analysis of the in-pixel IQ data phase

$$\underline{\widehat{\xi}}(z) = \left.\frac{\lambda}{2\pi}\mathcal{F}_t\left\{\Phi(z,t)\right\}\right|_{\omega_{\mathrm{M}}} \,, \tag{9}$$

that contains the amplitude and phase of the motion.

D. Model analysis

A derivation of the estimation scheme is not possible from the signal model (6) without simplifications [8]. For further analysis, the effect of motion in the frequency domain is investigated. The Fourier-transform with respect to fast and slow time is denoted as the complex Doppler-spectrum

$$U(k_z,\omega) = \int_{-\infty}^{\infty}\int_{-\infty}^{\infty} u_{\mathrm{ref}}(g(z,t))\,\mathrm{e}^{-\mathrm{j}k_z z}\,\mathrm{e}^{-\mathrm{j}\omega t}\,\mathrm{d}z\,\mathrm{d}t \tag{10}$$

$$= \frac{1}{2\pi}\int_{-\infty}^{\infty} U_{\mathrm{ref}}(l_z)\, P(k_z, l_z, \omega)\,\mathrm{d}l_z \,. \tag{11}$$

It arises from a linear operation in the frequency domain on the Fourier-transform of the reference configuration $U_{\text{ref}}(l_z)$ with a function describing the spread of energy due to motion

$$P(k_z, l_z, \omega) = \mathcal{F}_t \left\{ \mathcal{F}_z \left\{ \mathrm{e}^{\mathrm{j} l_z\, g(z,t)} \right\} \right\} .$$

This function simplifies if the motion is spatially homogeneous, i. e., $\xi(z)=$const. and of the same phase, e. g., $\varphi_{\mathrm{M}}=0$

$$P(k_z, l_z, \omega) = 2\pi\, \delta(k_z - l_z)\, \mathcal{F}_t \left\{ \mathrm{e}^{\mathrm{j} k_z\, \xi_0\, \sin(\omega_{\mathrm{M}}\, t)} \right\} \tag{12}$$

$$\Rightarrow U(k_z, \omega) = U_{\text{ref}}(k_z)\, \widetilde{P}(k_z, \omega) \tag{13}$$

with the specific complex Doppler-spectrum

$$\begin{aligned} \widetilde{P}(k_z, \omega) &= \mathcal{F}_t \left\{ \mathrm{e}^{\mathrm{j} k_z\, \xi_0\, \sin(\omega_{\mathrm{M}}\, t)} \right\} \qquad (14) \\ &= \mathrm{J}_0(k_z\, \xi_0)\, \delta(\omega) \\ &\quad + \sum_{n=1}^{\infty} \mathrm{J}_n(k_z\, \xi_0)\, \left[\delta(\omega - n\, \omega_{\mathrm{M}}) + \delta(\omega + n\, \omega_{\mathrm{M}}) \right] , \end{aligned}$$

and with $J_n(\cdot)$ as the Bessel function of the first kind of order n. Hence, the Fourier-transform of the A-scan with homogeneous harmonic motion, compatible to derivations of the conventional estimator, is

$$E(k_z, \omega) = S_{\text{t}}(k_z)\, U_{\text{ref}}(k_z)\, \widetilde{P}(k_z, \omega) + N(k_z, \omega) . \tag{15}$$

The observation that a harmonic motion generates higher harmonics in the Doppler-Spectrum has early been made and used by [12]–[15] and novel Doppler estimators have been developed based on the Doppler-spectrum for linear motion in [16], [17]. There, the Doppler-spectrum of linear and spatially homogeneous motion is calculated as

$$\widetilde{P}_{\text{lin}}(k_z, \omega) = 2\pi\, \delta(k_z - v\, \omega) \tag{16}$$

with v being the flow velocity. The comparison of (14) with (16) reveals the different characteristic between linear and harmonic motion: Contrary to classical Doppler [16], the harmonic motion leads to a spread of the energy of every spatial frequency k_z to discrete slow-time frequencies $n\, \omega_{\mathrm{M}}$ in the Doppler-spectrum.

E. Resulting findings and algorithm improvements

Due to the energy spread over the entire spectrum, sampling in slow-time must be fast enough ($f_F \gg 2\, f_M$) to consider the sampling theorem sufficiently fulfilled [18]. However, as $J_n(\cdot)$ rapidly decreases with n, the energy is concentrated at the lower frequencies. More important, almost no motion-related energy is at intermediate frequencies $\hat{E}(k_z, \omega \neq n\, \omega_{\mathrm{M}}) \approx N(k_z, \omega \neq n\, \omega_{\mathrm{M}})$, with $n \in \mathbb{N}$. Hence, this can be used for determination of SNR and for a prefilter (PF) setting $\hat{E}(k_z, \omega \neq n\, \omega_{\mathrm{M}}) = 0$ to suppress noise and interfering motion not associated with the motion at ω_{M} to be detected.

From classical Doppler theory it is known that phase-based motion estimators perform best on continuous wave, i.e., narrow-band, signals to achieve the lowest variance of the estimate. Here, it can be verified that the conventional motion estimator perfectly performs in case of ideal impulse excitation of a moving point scatterer, i. e., $u(z,t)=\delta(g(z,t)) \wedge s_{\mathrm{t}}=\delta(t)$. However, realistic motion is spatially smooth and is expected to approximately match the case of (15). This motivates to perform the motion estimation in a narrow band by demodulating to a frequency within the transducer bandwidth and filtering with a suitable low-pass filter $h(t)$ with a passband significantly smaller than the transducer bandwidth. To exploit all spectral energy of a typical wide-band ultrasonic pulse, multiple estimates obtained inside the transducer bandwidth can be combined, e. g., by averaging multiple estimates, thereby suppressing uncorrelated noise.

Motion estimation in different frequency bands is therefore performed with modifications: The first is phase-based motion estimation on *narrow-band* data, by reducing the RF data bandwidth with $h(t)$ by a factor of B. The second is demodulation to B equally spaced frequencies and performing B *multi-band* estimations on a reduced bandwidth of $B^{-1}\cdot 100\%$, such that the full bandwidth of the RF data is exploited. These modifications are tested with and without the PF. The error metric is the mean absolute error (MAE) between the estimate and the actual motion calculated over the motion profile between 12–28 mm. The SNR is varied between 0–80 dB. To investigate the influence of the bandwidth parameter B, it was varied between 1 and 10.

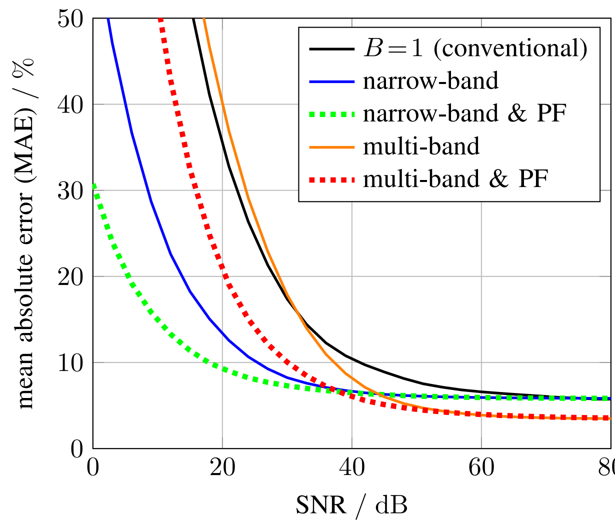

Fig. 1. Mean absolute error relative to the peak displacement of 5 µm for conventional and modified estimators using $B = 10$ bands with and without a prefilter (PF).

III. Results

Fig. 1 shows the MAE over SNR which was calculated on a single A-scan realization but averaged over 100 different realizations of additive white Gaussian noise. At an SNR better than 60 dB, the estimate does not improve further, so that it s biased estimator for a fixed scatterer realization. Towards lower SNR, the estimates on narrow-band data outperform the conventional estimate significantly and preprocessing is particularly advantageous for low SNR. However, with good

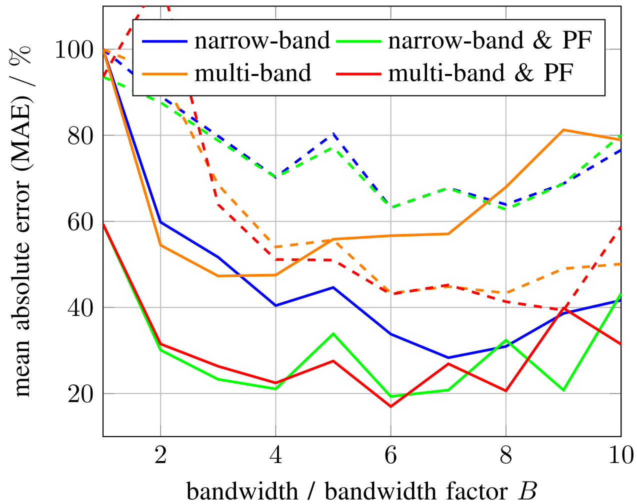

Fig. 2. Mean absolute error relative to the conventional estimator MAE for an SNR of 60 dB (dashed lines, conventional MAE 302 nm) and 30 dB (solid lines, conventional MAE 1.13 µm).

SNR, the multi-band estimation is advantageous and a PF has not a significant influence.

For a single realization of the scatterer distribution and a single realization of the noise, the reduction of MAE compared to the conventional estimate is depicted in Fig. 2 for good (60 dB) and moderate (30 dB) SNR. Almost all modified estimates outperform the conventional estimate. The MAE reduction is larger for low SNR. Additionally, for this scenario the optimum estimator is the multi-band processing with a PF using $B = 4$–8 Bands.

IV. Discussion & Conclusion

A theoretical analysis has shown that the RF data of harmonically vibrating tissue exhibit different characteristics than in typical Doppler applications. It was deduced that motion estimation should be performed on narrow-band data, which was not discussed so far. The results indicate that the data that were not processed in a narrow band estimate can still be used to improve the estimate by averaging from different band ranges. Thus, a significant increase in estimator performance can be achieved with little or no additional computational effort. A prefilter has shown to be suitable for suppressing interference noise. The ability to suppress interfering motion can prospectively be analyzed. An analysis of all RF data and motion related parameters is necessary to fully exploit the potential of the presented methods.

The simulation data also show that the phase-based estimation has a significant residual error independent of the SNR. Therefore, further improvements may only be possible by deriving estimators on a more sophisticated model of motion in RF data. This is especially important for MMUS, where particularly small displacements are to be estimated.

References

[1] J. Oh, M. D. Feldman, J. Kim, C. Condit, S. Emelianov, and T. E. Milner, “Detection of magnetic nanoparticles in tissue using magneto-motive ultrasound,” *Nanotechnol.*, vol. 17, no. 16, pp. 4183–4190, 2006.

[2] A. L. Oldenburg, F. J.-J. Toublan, K. S. Suslick, A. Wei, and S. A. Boppart, “Magnetomotive contrast for in vivo optical coherence tomography,” *Opt. Express*, vol. 13, no. 17, pp. 6597–6614, 2005.

[3] A. L. Oldenburg, V. Crecea, S. A. Rinne, and S. A. Boppart, “Phase-resolved magnetomotive OCT for imaging nanomolar concentrations of magnetic nanoparticles in tissues,” *Opt. Express*, vol. 16, no. 15, pp. 11 525–11 539, 2008.

[4] M. Mehrmohammadi, J. Oh, S. R. Aglyamov, A. B. Karpiouk, and S. Y. Emelianov, “Pulsed magneto-acoustic imaging,” in *Proc. 2009 IEEE Int. Conf. Eng. Medicine and Biol. Soc. (EMBC)*, 2009, pp. 4771–4774.

[5] A. L. Oldenburg, W. Luo, and S. A. Boppart, “High-resolution in vivo nanoparticle imaging using magnetomotive optical coherence tomography,” in *Proc. SPIE 6097, Opt. Mol. Probes for Biomedical Appl.*, vol. 609702, 2006.

[6] M. Evertsson, M. Cinthio, S. Fredriksson, F. Olsson, H. W. Persson, and T. Jansson, “Frequency- and phase-sensitive magnetomotive ultrasound imaging of superparamagnetic iron oxide nanoparticles,” *IEEE Trans. Ultrason., Ferroelectr., Freq. Control*, vol. 60, no. 3, pp. 481–491, 2013.

[7] A. G. Pope, G. Wu, F. Y. McWhorter, E. P. Merricks, T. C. Nichols, T. J. Czernuszewicz, C. M. Gallippi, and A. L. Oldenburg, “Contrast-enhanced imaging of SPIO-labeled platelets using magnetomotive ultrasound,” *Phys. Med. Biol.*, vol. 58, no. 20, pp. 7277–7290, 2013.

[8] T. C. Kranemann, T. Ersepke, and G. Schmitz, “Real-time magnetomotive ultrasound imaging using a recursive estimator,” in *Proc. 2018 IEEE Int. Ultrason. Symp. (IUS)*, 2018.

[9] M. M. Hossain, B. E. Levy, D. Thapa, A. L. Oldenburg, and C. M. Gallippi, “Blind source separation-based motion detector for imaging superparamagnetic iron oxide (SPIO) particles in magnetomotive ultrasound imaging,” *IEEE Trans. Med. Imag.*, vol. 37, no. 10, pp. 2356–2366, 2018.

[10] T. Ersepke, T. C. Kranemann, and G. Schmitz, “On the performance of time domain displacement estimators for magnetomotive ultrasound imaging,” *IEEE Trans. Ultrason., Ferroelectr., Freq. Control*, 2019.

[11] J. A. Jensen, “Field: A program for simulating ultrasound systems,” *Medical & Biol. Eng. & Comput.*, vol. 34, no. 1, pp. 351–353, 1996, 10th Nordic-Baltic Conference on Biomedical Imaging.

[12] J. Holen, R. C. Waag, and R. Gramiak, “Representations of rapidly oscillating structures on the Doppler display,” *Ultrasound in Medicine & Biol.*, vol. 11, no. 2, pp. 267–272, 1985.

[13] A. Nowicki and A. Marciniak, “Detection of wall vibrations by means of cepstrum analysis,” *Ultrason. Imag.*, vol. 11, no. 4, pp. 273–282, 1989.

[14] Y. Yamakoshi, J. Sato, and T. Sato, “Ultrasonic imaging of internal vibration of soft tissue under forced vibration,” *IEEE Trans. Ultrason., Ferroelectr., Freq. Control*, vol. 37, no. 2, pp. 45–53, mar 1990.

[15] S. Huang, R. M. Lerner, and K. J. Parker, “Time domain Doppler estimators of the amplitude of vibrating targets,” *J. Acoustical Soc. America*, vol. 91, no. 2, pp. 965–974, 1992.

[16] T. Loupas and R. W. Gill, “Multifrequency Doppler: Improving the quality of spectral estimation by making full use of the information present in the backscattered RF echoes,” *IEEE Trans. Ultrason., Ferroelectr., Freq. Control*, vol. 41, no. 4, pp. 522–531, 1994.

[17] T. Loupas, J. T. Powers, and R. W. Gill, “An axial velocity estimator for ultrasound blood flow imaging, based on a full evaluation of the Doppler equation by means of a two-dimensional autocorrelation approach,” *IEEE Trans. Ultrason., Ferroelectr., Freq. Control*, vol. 42, no. 4, pp. 672–688, 1995.

[18] S. Bergner, T. Moller, D. Weiskopf, and D. J. Muraki, “A spectral analysis of function composition and its implications for sampling in direct volume visualization,” *IEEE Trans. Vis. Comput. Graphics*, vol. 12, no. 5, pp. 1353–1360, 2006.